Journal of Applied Polymer Science

In situ fast polymerization of graphene nanosheets-filled poly(methyl methacrylate) nanocomposites

Lan-Ying Zhang, Yang-Fei Zhang
Department of Materials Science and Engineering, College of Engineering, Peking University, Beijing 100871, China
Correspondence to: Y.-F. Zhang (E-mail: zhangyangfei@pku.edu.cn)

ABSTRACT: A series of graphene nanosheets-filled poly(methyl methacrylate) nanocomposites (GNS/PMMA) is successfully prepared by an *in situ* fast polymerization method with graphene weight fractions from 0.1 to 2.0 wt %. *In situ* polymerization is effective in well dispersing of GNS in matrixes and suitable for both low and high content of GNS. The synthesis processes of polymer composites could be simplified and fast by using industrial grade graphene. The GNS fillers are found to disperse homogeneously in the PMMA matrix. The maximum electrical conductivity of the composites achieves 0.57 S m^{-1}, with an extremely low percolation threshold of 0.3 wt %. The electrical conductivities are further predicted by percolation theory and found to agree well with the experimental results. The results indicate that the microstructures, thermal, electrical, and mechanical properties of PMMA polymer are significantly improved by adding a low amount of graphene nanosheets. © 2016 Wiley Periodicals, Inc. J. Appl. Polym. Sci. **2016**, *133*, 43423.

KEYWORDS: composites; graphene and fullerenes; microscopy; nanotubes; properties and characterization

Received 22 October 2015; accepted 7 January 2016
DOI: 10.1002/app.43423

INTRODUCTION

Graphene-filled polymer nanocomposites have attracted significant research interest in materials science and have great potential in the engineering applications of sensors, super capacitors, batteries, conductive films, and thermal interfaces.[1–3] Attributing to the unique structure and excellent properties such as electrical conductivity, mechanical flexibility, thermal conductivity, and optical transparent, the addition of graphene nanosheet (GNS) has been found to improve the thermal, electrical and mechanical properties of various polymers, including polystyrene,[4] polyurethane,[5] epoxy,[6] polyethylene,[7] etc.

Poly(methyl methacrylate) (PMMA) is one of the most important engineering thermoplastics and widely used as a matrix in polymer composites, with excellent performances of colorless, high light transmittance, low birefringence, good impact resistance and strong resistance to chemical and weathering corrosion. Different nanoscale fillers such as carbon black,[8] silica nanoparticles,[9] carbon nanotubes,[10] carbon nanofibers,[11] and graphite nanoplatelets,[12] have been applied to reinforce the performances of PMMA polymer. Because of the special structure of two dimensional platelet and extraordinary properties, GNS has been considered to be an excellent nanoscale filler to improve the thermal, electrical and mechanical properties of PMMA polymer.[13–17]

Several preparation methods of solution mixing,[18] melt blending,[19] self-assembly,[20] and in situ polymerization[21–25] have been developed to fabricate GNS/PMMA composites. To achieve high performance nanocomposites, the homogeneous dispersion of GNS in polymer matrix and strong interface between GNS and polymer are crucial.[6,26] *In situ* polymerization method has been proved to be more effective in well dispersing of GNS in matrixes and suitable for both low and high content of GNS, attributing to the polymer growing in the presence of nanoscale fillers.[27–29]

However, most of the GNS nanoscale fillers in previous studies of GNS/PMMA composites were prepared by the reduction of graphene oxide and graphite oxide during the *in situ* polymerization process. With the development of highly efficient graphite layer exfoliation technique and industrial grade graphene,[1,30,31] the synthesis processes of polymer composites could be simplified and fast, which is benefit for the time and cost reduction. Attributing to the uniform morphology, controlled quality, large quantity, and high purity of preproduced GNS, the microstructures and properties of GNS-filled polymer composites could be significantly improved.

In this study, a series of preproduced GNS-filled PMMA nanocomposites was prepared by an *in situ* fast polymerization method. The thermal, electrical and mechanical properties were experimentally measured and discussed according to the microstructures. The electrical conductivities of GNS-filled PMMA composites were further predicted by classical percolation theory and compared with the experimental results.

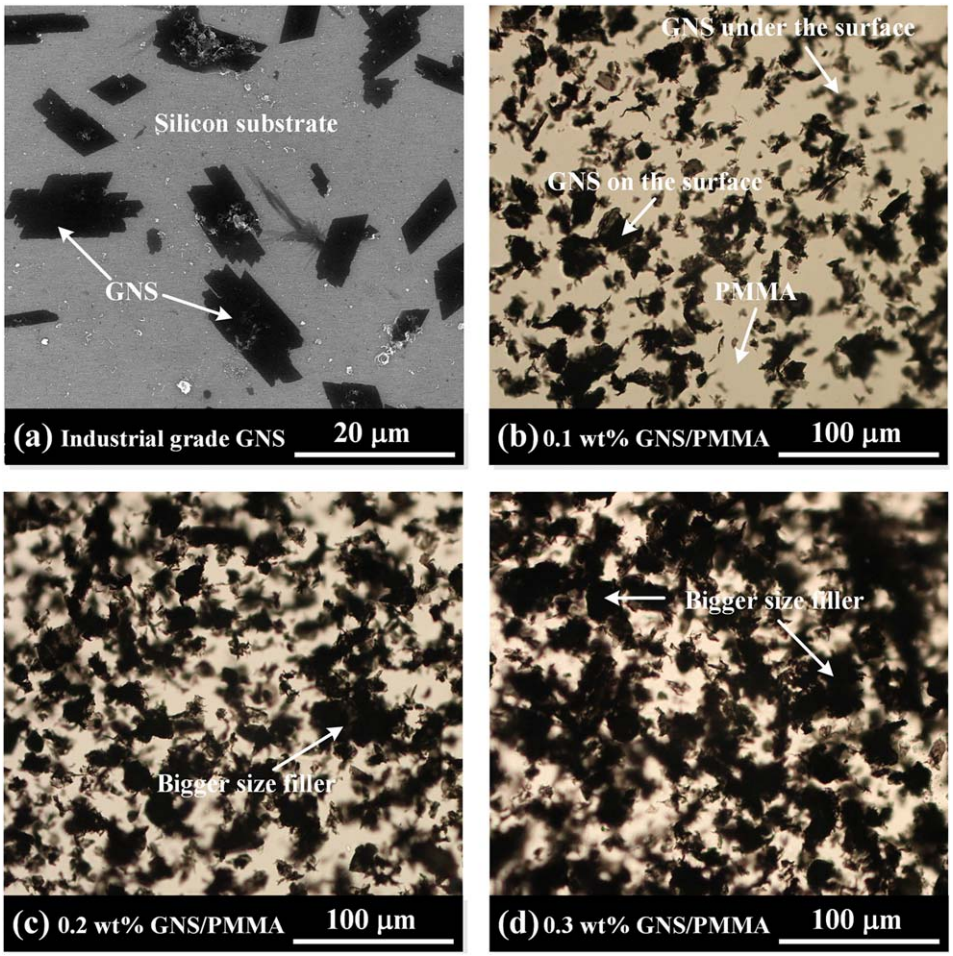

Figure 1. SEM photograph of (a) industrial grade GNS and TPM photographs of composites with GNS contents of (b) 0.1 wt %, (c) 0.2 wt %, and (d) 0.3 wt %. [Color figure can be viewed in the online issue, which is available at wileyonlinelibrary.com.]

EXPERIMENTAL

Materials

The industrial grade GNS with a diameter of $5-15$ μm and thickness of $1-2$ nm was supplied by Morsh Co. Ltd, China. The GNS was dispersed in absolute ethyl alcohol and then deposited on the silicon substrate. The average diameter of GNS was measured by an image analysis program on SEM images. As shown in Figure 1(a), the industrial grade GNS deposited on silicon substrate is found to be from several hundred nanometers to tens micrometers, with an average diameter of 7.3 μm calculated by 851 nanosheets. The GNS was washed by acetone and dried for 12 h at 80 °C under vacuum before added to the solution. The monomer, methyl methacrylate (MMA) with a purity of >99.0 wt % and relative molecular mass of 100.12 was supplied by Yili Fine Chemical, China. Benzoyl peroxide (BPO) with a purity of >99.0 wt % was used as the initiator and supplied by Guanghua Chemical, China. Other chemicals were of analytical grade.

Preparation of GNS/PMMA Nanocomposites

The GNS/PMMA nanocomposites were prepared by an *in situ* fast polymerization method. 50 mg BPO was completely dissolved in 30 g MMA monomer before GNS was added to the solution. For homogeneous dispersion, the mixture was sonicated in an ultrasonic cleaner under frequency of 56 kHz and power of 100 W and simultaneously mixed by a mechanical stirrer for 15 min, and then heated to 85, 80, 78, 76, 74, 72, 70 °C in a thermostatic oil bath to promote prepolymerization, corresponding to the GNS weight fractions of 0, 0.1, 0.2, 0.3, 0.5, 1.0, and 2.0 wt %, respectively. These seven different prepolymerization temperatures are used to control the viscosities of mixtures with different GNS content and guarantee enough time for ultrasonic and mechanical stirring. The reaction mixture was maintained with mechanical stirring for 30 min before the mixture became few viscous, and then cooling to room temperature quickly. To achieve fully polymerization, the mixture was heated to 50 °C under vacuum for 12 h. The film samples for TMP, four point probe, and nanoindentation tests are prepared by spin coating method with a thickness of about 100 μm, while the bulk samples for other tests are prepared by casting in molds corresponding to testing standards.

Characterization

The microstructures of the composites were observed by a transmitted polarization microscope (TPM) (59XC-PC, Shanghai Optical Co.) with halogen lamp of 765 lumens and a scanning electron microscope (SEM) (S4800, Hitachi Co.) with secondary

electron detector, accelerating voltage of 5 KV and current of 10 μA.

The thermal stability was measured by a thermogravimetric analysis instrument (TGA) (TGA4000, PerkinElmer Co.) under nitrogen, with the temperature range from room temperature to 600 °C and heating rate of 20 °C min^{-1}. The phase transition temperatures were measured by a differential scanning calorimetry instrument (DSC) (DSC8000, PerkinElmer Co.) at a scanning rate of 10 °C min^{-1}.

The electrical conductivities of the composites with GNS content equal and beyond 0.3 wt % were measured by a four point probe meter (RTS-8, Guangzhou Probe Co.) combined with a Keithley 2400 source meter, ranging from 10^{-8} to 10^{3} S m^{-1}. The electrical conductivities of the composites with GNS content equal and less than 0.2 wt % were measured by voltage-current method and performed on an insulation resistance tester (ZC-90, Taiou Co.).

The elastic modulus and tensile strength were measured by a universal material testing machine (5969, Instron Co.) at a loading rate of 1 mm min^{-1}, following standard ISO 527-2:2012. The Rockwell hardness was measured by a Rockwell hardness testing machine (HR-150D, Laihua Co.) with a steel ball of 6.35 mm diameter, following standard ISO 2039-2:2000. The nanoindentation hardness was measured by a Tribo Indentor (TI, Hysitron Co.) with a Berkovich diamond tip of 100 nm, following standard ISO 14577:2002. The notched Izod impact strength was measured by a pendulum impact machine (XJU-5.5J, Desheng Co.) with a pendulum energy of 5.5 J, following standard ISO 180:2000. Each test was repeated 6-10 times to obtain average values with error bars by standard deviations.

RESULTS AND DISCUSSION

Microstructures

As shown in Figure 1, the GNS fillers are found to be homogenously dispersed in the PMMA matrix by TPM observation, attributing to the low viscosity of MMA monomers and *in situ* polymerization of the monomers on the surfaces of GNS. The homogeneous dispersion of nanoscale fillers in the matrix can provide superior microstructures and performances. However, the thickness of TMP sample (100 μm) is much larger than the thickness of GNS (few nanometers), so the GNS fillers under TMP sample surface are unfocused, overlapped and showed as indistinct dark area, which seems to increase the GNS areas. A few agglomerates of GNS behaving like bigger size fillers are observed and dispersed homogenously in the PMMA matrix as the same as GNS. The sizes of GNS agglomerates are found to be enlarged with the GNS content. When the GNS content is beyond 0.3 wt %, the GNS fillers begin to connect each other.

The SEM observation on the middle of fracture surfaces after impact tests is shown in Figure 2. The surfaces are relatively flat and smooth for low GNS content less than 0.3 wt %. The enhanced interfacial interaction between GNS and matrix is attributed to the excellent fluidity and spreading of the MMA monomers during ultrasonic and mechanical stirring processes and *in situ* polymerization of the monomers on the surfaces of GNS. For higher GNS content beyond 0.5 wt %, micro pores and voids appear on the impact fracture surface, as well as the crumpled, wrinkled and folded GNS. It is also observed on the fracture surfaces after tensile tests [24], mainly due to the size enlarging of GNS agglomerates, in which MMA monomers are difficult to flow and coat on the surfaces of each GNS. The similar morphology has also been observed in GNS/nylon-6[32] and GNS/polyethylene composites.[33]

Thermal Stability and Phase Transitions

Figure 3 shows the TGA curves of nonoxidative thermal degradation of neat PMMA and GNS/PMMA composites at the temperature range of 50 − 600 °C. Their 5% weight loss temperatures (T_d's) are summarized in Table I.

For the composites with GNS content less than 1.0 wt %, the thermal degradation temperatures are slightly affected. However, the T_d of GNS/PMMA composite with 2.0 wt % GNS shows a significant improvement, 41.4 °C higher than that of neat PMMA, which illustrates that GNS can substantially improve the thermal stability of PMMA polymer by the *in situ* fast polymerization method. The enhancement of thermal degradation temperature is more obvious for reduced graphene oxide-filled PMMA composites.[28,29]

The phase transition temperatures of neat PMMA and GNS/PMMA composites are measured by DSC tests. To eliminate the generated complex thermal history of the composites during solvent evaporation and drying, the first cooling and second heating DSC traces were used to determine the glass transition temperatures T_g. As presented in Table I, the T_g of the composites is gradually decreased with the addition of GNS. The T_g of the composite with 2.0 wt % GNS is 100.5 °C, 9.1 °C lower than that of neat PMMA. The reinforcement of thermal stability and phase transitions is attributed to the interfacial interactions between the GNS fillers and the PMMA matrix. Compared with other physical blending method such as solvent processes, chemical blending processes such as *in situ* polymerization can yield strong covalent bonds and provide enough interaction at the interfaces.[34]

Electrical Conductivity

Figure 4 shows a marked percolation behavior of electrical conductivity varying with GNS content. The conductivity of GRN/PMMA composites increases rapidly before the critical percolation threshold of 0.3 wt %, from 1.75 × 10 − 15 S m^{-1} to 3.71 × 10-4 S m^{-1}, and then increases to 0.57 S m^{-1} at GNS content of 2.0 wt %. The electrical properties are much better than graphite nanoplatelets-filled PMMA composites with much lower critical percolation threshold and higher conductivity.[27] According to the results of 0.3 wt % GNS/PMMA composite, it is believed that a conductive network of GNS electron transport paths is formed inside the material, in accordance with the TPM observation in Figure 1. The excellent electrical properties of GNS/PMMA composites are also strongly dependent on the homogenously distribution of the conductive GNS fillers in the PMMA polymer matrix. The extremely low percolation threshold and relatively high electrical conductivity can be attributed to the high aspect ratio, large surface area and high conductivity of GNS fillers as well as the enhanced interfacial interaction between GNS and PMMA interface.[35,36]

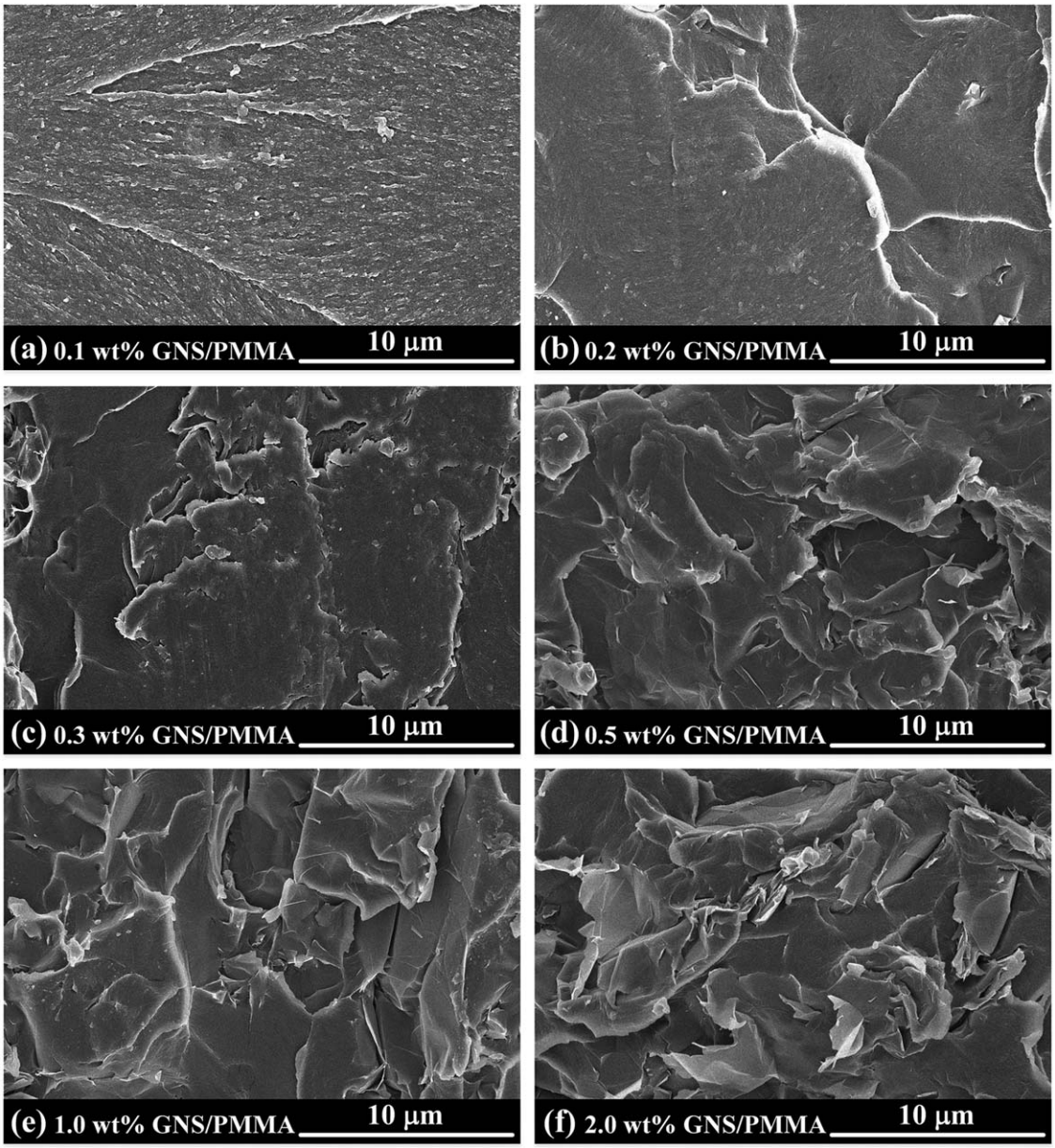

Figure 2. SEM photographs of impact fracture surfaces of composites with GNS contents of (a) 0.1 wt %, (b) 0.2 wt %, (c) 0.3 wt %, (d) 0.5 wt %, (e) 1.0 wt %, and (f) 2.0 wt %.

The conductivity of the composites can be further predicted in terms of percolation theory, based on the conductive network formed by electron transport paths through the volume of the sample. According to the classical percolation theory,[37] the electrical conductivity of the composites σ can be calculated by the following equation:

$$\sigma = \sigma_f (v - v_c)^t \quad (1)$$

$$v = \frac{w_f}{\rho_f} \Big/ \left(\frac{1 - w_f}{\rho_m} + \frac{w_f}{\rho_f} \right) \quad (2)$$

where σ_f is the electrical conductivity of GNS filler (64 mS cm^{-1}, measured by four point probe method[38]), v is the volume fraction of GNS filler, v_c is the critical percolation volume fraction (0.17 vol %, corresponding to 0.3 wt %), t is the critical exponent reflecting the system dimensionality of the composites, w_f is the weight fraction of GNS filler, ρ_f is the density of GNS filler (2.1 g cm^{-3}), ρ_m is the density of PMMA matrix (1.2 g cm^{-3}). The critical exponent t depends only on the dimensionality of the composites, and follows a power law dependence of approximately 2 in a three dimensional system and $1 - 1.3$ in a two-dimensional system. The experimental results show that the electrical conductivity follows a power law dependence of approximately $t = 1 - 1.3$, indicating the presence of a two-dimensional conductive network on the surface of composite. [35]

Mechanical Properties

Elastic Modulus and Tensile Strength

Figure 5 shows the elastic modulus and tensile strength of GNS/PMMA composites measured by tensile tests. It can be found

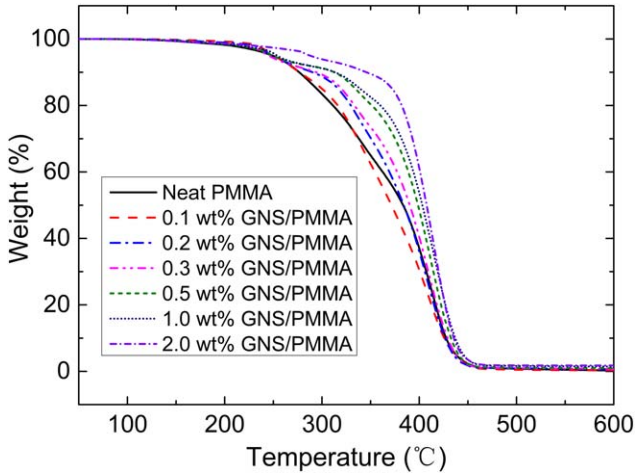

Figure 3. TGA curves of GNS/PMMA composites. [Color figure can be viewed in the online issue, which is available at wileyonlinelibrary.com.]

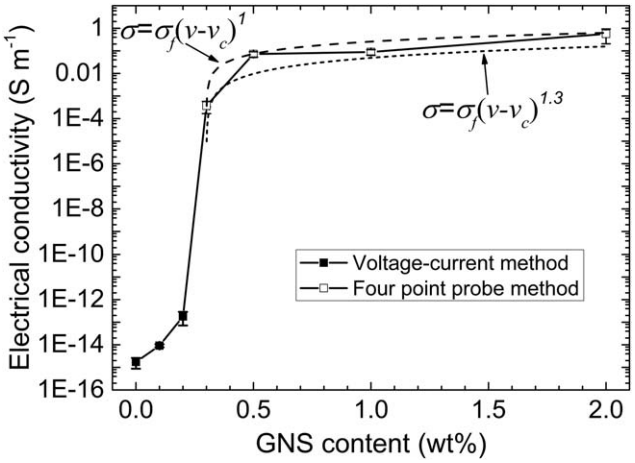

Figure 4. Electrical conductivity of GNS/PMMA composites.

that a low addition of GNS leads to great improvements of modulus and tensile strength, indicating a marked increase in the stiffness of the composites. The modulus achieves the maximum value of 3.11 GPa as the GNS content increases to 0.3 wt %, improving the modulus of neat PMMA about 14%. The tensile strength of the composites shows a similar behavior and achieves the maximum value of 42.73 MPa at the GNS content of 0.3 wt %, improving the tensile strength of neat PMMA about 41%.

However, higher GNS contents beyond 0.5 wt % lead to deterioration of elastic modulus and tensile strength, due to the poor stress transfer. The load transfer depends on the interfacial shear stress between the filler and the matrix. The main mechanisms of load transfer from matrix to filler are micromechanical interlocking, chemical bonding, and the Van Der Waals force.[39] The loading force can be easily transferred by the enhanced interfacial interactions of chemical bonding between GNS fillers and PMMA matrix supplied by *in situ* polymerization and the high modulus, high strength and high aspect ratio of GNS filler. GNS fillers could contact each other by plane to plane, edge to edge and edge to plane when the conductive network is formed at the GNS content of 0.3 wt %. For higher GNS contents beyond 0.5 wt %, the appearance and increase of micro pores and voids, as shown in Figure 2 and discussed in the *Microstructures* section, weaken the interfaces of the GNS filler and the PMMA matrix as well as the load transfer performance.

Table I. TGA Traces and DSC Phase Transitions of GNS/PMMA Composites

Sample	T_d (°C)[a]	T_g (°C)[b]
Neat PMMA	251.5	109.6
0.1 wt % GNS/PMMA	252.9	105.9
0.2 wt % GNS/PMMA	253.1	104.7
0.3 wt % GNS/PMMA	247.1	103.9
0.5 wt % GNS/PMMA	251.5	101.4
1.0 wt % GNS/PMMA	254.9	101.1
2.0 wt % GNS/PMMA	292.9	100.5

[a] The temperatures at 5% weight loss of the samples under nitrogen were measured by TGA heating experiments at a rate of 20 °C min^{-1}.
[b] The glass transition temperatures of the samples under a nitrogen atmosphere were measured by DSC at a scanning rate of 10 °C min^{-1}.

Hardness

The variation of hardness with GNS content for Rockwell hardness tests and nanoindentaion tests are similar, as shown in Figure 6. It is found that a low addition of GNS leads to great improvements of hardness, indicating an excellent resistant for solid matter with a compressive force. The Rockwell hardness achieves the maximum value of 111.2 HRc as the GNS content increases to 0.3 wt %, improving the hardness of neat PMMA about 5%. Compared with Rockwell hardness, the nanoindentation hardness reflects much more localized behaviors and achieves the maximum value of 328.9 MPa as the GNS content increases to 0.3 wt %, improving the hardness of neat PMMA about 40%. The larger value is possibly due to the fact that elastic deformation is considered during the nanoindentation test and GNS generates more elastic deformation than plastic deformation.[40] However, higher GNS contents beyond 0.5 wt % lead to deterioration of both Rockwell hardness and nanoindentation

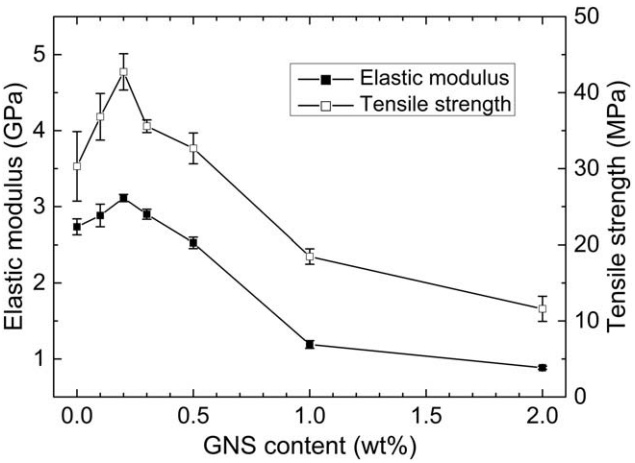

Figure 5. Elastic modulus and tensile strength of GNS/PMMA composites.

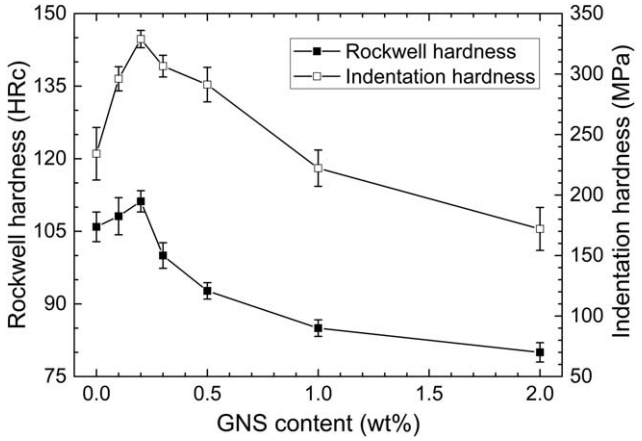

Figure 6. Rockwell hardness and nanoindentation hardness of GNS/PMMA composites.

hardness, the same as the modulus and strength. It is attributed to the fact that the appearance and increase of micro pores and voids weaken the interfaces of the GNS filler and the PMMA matrix and the load transfer performance.

Impact Strength

As shown in Figure 7, the impact strength is slightly decreased by adding a low content of GNS, then it follows an approximately linear increase with the GNS content, illustrating that more energies could be dissipated in the composites before the failures occur. The impact strength of PMMA polymer is significantly improved by adding 2.0 wt % GNS and achieves a high value of 12.89 KJ m^{-2}, about 194% larger than that of neat PMMA. It is attributed to the excellent mechanical properties of GNS filler and strong interfacial interactions between GNS filler and PMMA matrix, contributing to better toughening effect on the PMMA matrix.

CONCLUSIONS

A series of GNS/PMMA nanocomposites was successfully prepared by an *in situ* fast polymerization method. GNS fillers are found to be homogenously dispersed in the PMMA matrix.

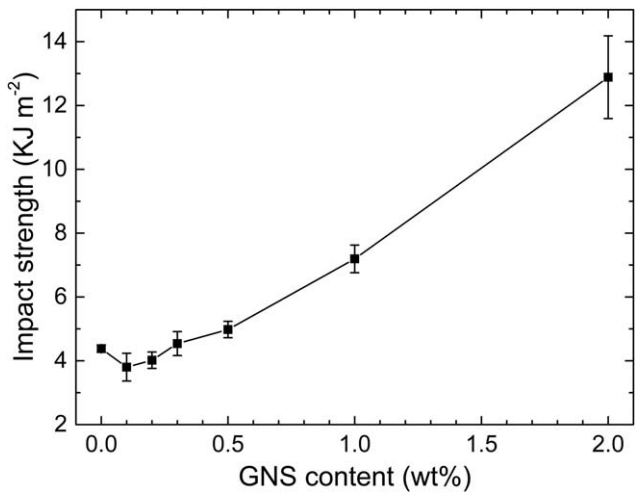

Figure 7. Impact strength of GNS/PMMA composites.

The experimental results show that GNS can substantially improve the thermal stability of PMMA polymer and decrease the glass transition temperatures. The maximum electrical conductivity of the composites was 0.57 S m^{-1}, with an extremely low percolation threshold of 0.3 wt %. The electrical conductivities predicted by classical percolation theory are found to agree well with the experimental results. At the critical threshold of 0.3 wt %, the elastic modulus, tensile strength, Rockwell hardness and nanoindentation hardness achieve the maximum values, about 14%, 41%, 5%, and 40% larger than those of neat PMMA, respectively. The impact strength of PMMA polymer is significantly improved by adding 2.0 wt % GNS and achieves a high value of 12.89 KJ m^{-2}, about 194% larger than that of neat PMMA. The results indicate that the microstructures and properties of PMMA polymer can be significantly improved by adding a low amount of graphene nanosheets.

ACKNOWLEDGMENTS

This work is supported by the National Natural Science Foundation of China (No. 11202005, No. 51203003, No.51573003) and Beijing Natural Science Foundation (No. 3122019).

REFERENCES

1. Zhu, J. H.; Chen, M. J.; He, Q. L.; Shao, L.; Wei, S. Y.; Guo, Z. *RSC. Adv.* **2013**, *3*, 22790.
2. Kuilla, T.; Bhadra, S.; Yao, D.; Kim, N. H.; Bose, S.; Lee, J. H. *Prog. Polym. Sci.* **2010**, *35*, 1350.
3. Huang, X.; Qi, X. Y.; Boey, F.; Zhang, H. *Chem. Soc. Rev.* **2012**, *41*, 666.
4. Stankovich, S.; Dikin, D. A.; Dommett, G. H. B.; Kohlhaas, K. M.; Zimney, E. J.; Stach, E. A.; Piner, R. D.; Nguyen, S. T.; Ruoff, R. S. *Nature* **2006**, *442*, 282.
5. Yadav, S. K.; Yoo, H. J.; Cho, J. W. *J. Polym. Sci. Part B: Pol. Phys.* **2013**, *51*, 39.
6. Tang, L. C.; Wan, Y. J.; Yan, D.; Pei, Y. B.; Zhao, L.; Li, Y. B.; Wu, L. B.; Jiang, J. X.; Lai, G. Q. *Carbon* **2013**, *60*, 16.
7. Pokharel, P.; Bae, H.; Lim, J. G.; Lee, K. Y.; Choi, S. *J. Appl. Polym. Sci.* **2015**, *132*, 42073.
8. Brigandi, P. J.; Cogen, J. M.; Wolf, C. A.; Reffner, J. R.; Pearson, R. A. *J. Appl. Polym. Sci.* **2015**, *132*, 42134.
9. Chen, Y. Z.; Zhang, Z. P.; Yu, J.; Guo, Z. X. *J. Polym. Sci. Part B: Pol. Phys.* **2009**, *47*, 1211.
10. Luo, J. T.; Wen, H. C.; Wu, W. F.; Chou, C. P. *Polym. Compos.* **2008**, *29*, 1285.
11. Helena, V. R.; Iluminada, R. P.; Ignacio, M. G. *J. Appl. Polym. Sci.* **2012**, *25*, 3228.
12. Zhang, L.; Zhu, J. Q.; Zhou, W. B.; Wang, J.; Wang, Y. *Energy* **2012**, *39*, 294.
13. Ramanathan, T.; Abdala, A. A.; Stankovich, S.; Dikin, D. A.; Herrera-Alonso, M.; Piner, R. D.; Adamson, D. H.; Schniepp, H. C.; Chen, X.; Ruoff, R. S.; Nguyen, S. T.; Aksay, I. A.; Prud-Homme, R. K.; Brinson, L. C. *Nat. Nanotechnol.* **2008**, *3*, 327.

14. Wang, J. C.; Hu, H. T.; Wang, X. B.; Xu, C. H.; Zhang, M.; Shang, Z. P. *J. Appl. Polym. Sci.* **2011**, *122*, 1866.
15. Valles, C.; Abdelkader, A. M.; Young, R. J.; Kinloch, I. A. *Compos. Sci Technol.* **2015**, *111*, 17.
16. Cai, D. Y.; Song, M. *J. Mater. Chem.* **2010**, *20*, 7906.
17. Verma, D.; Gope, P. C.; Shandilya, A.; Gupta, A. *T. Indian I. Metals* **2014**, *67*, 803.
18. Zeng, X. P.; Yang, J. J.; Yuan, W. X. *Eur. Polym. J.* **2012**, *48*, 1674.
19. Jiang, S. H.; Gui, Z.; Bao, C. L.; Dai, K.; Wang, X.; Zhou, K. Q.; Shi, Y. Q.; Lo, S. M.; Hu, Y. *Chem. Eng. J.* **2013**, *226*, 326.
20. Yang, J. T.; Yan, X. H.; Wu, M. J.; Chen, F.; Fei, Z. D.; Zhou, M. Q. *J. Nanopart. Res.* **2012**, *14*, 717.
21. Pramoda, K. P.; Hussain, H.; Koh, H. M.; Tan, H. R.; He, C. B. *J. Polym. Sci. Part A: Pol. Chem.* **2010**, *48*, 4262.
22. Yuan, X. Y.; Zou, L. L.; Liao, C. C.; Dai, J. W. *Express Polym. Lett.* **2012**, *6*, 847.
23. Hu, X. J.; Su, E. Q.; Zhu, B. C.; Jia, J. J.; Yao, P. H.; Bai, Y. X. *Compos. Sci. Technol.* **2014**, *97*, 6.
24. Wang, J. L.; Shi, Z. X.; Ge, Y.; Wang, Y.; Fan, J. C.; Yin, J. *Mater. Chem. Phys.* **2012**, *136*, 43.
25. Aldosari, M. A.; Othman, A. A.; Alsharaeh, E. H. *Molecules* **2013**, *18*, 3152.
26. Villar-Rodil, S.; Paredes, J. I.; Martinez-Alonso, A.; Tascon, J. M. D. *J. Mater. Chem.* **2009**, *19*, 3591.
27. Xu, K.; Erricolo, D.; Dutta, M.; Stroscio, M. A. *Superlattices Microstruct.* **2012**, *51*, 606.
28. Tripathi, S. N.; Saini, P.; Gupta, D.; Choudhary, V. *J. Mater. Sci.* **2013**, *48*, 6223.
29. Kuila, T.; Bose, S.; Khanra, P.; Kim, N. H.; Rhee, K. Y.; Lee, J. H. *Compos. Part A-Appl. S.* **2011**, *42*, 1856.
30. Stankovich, S.; Dikin, D. A.; Piner, R. D.; Kohlhaas, K. A.; Kleinhammes, A.; Jia, Y. *Carbon* **2007**, *45*, 1558.
31. Kyle, J. R.; Ozkan, C. S.; Ozkan, M. *Nanoscale* **2012**, *4*, 3807.
32. Xu, Z.; Gao, C. *Macromolecules* **2010**, *43*, 6716.
33. Fim, F. C.; Basso, N. R. S.; Graebin, A. P.; Azambuja, D. S.; Galland, G. B. *J. Appl. Polym. Sci.* **2013**, *128*, 2630.
34. Liao, K. H.; Aoyama, S.; Abdala, A. A.; Macosko, C. *Macromolecules* **2014**, *47*, 8311.
35. Liu, X.; Qin, Z. Y.; Dou, Z. J.; Liu, N.; Chen, L.; Zhu, M. F. *RSC. Adv.* **2014**, *4*, 23869.
36. Pang, H.; Chen, T.; Zhang, G. M.; Zeng, B. Q.; Li, Z. M. *Mater. Lett.* **2010**, *64*, 2226.
37. Stauffer, D.; Aharony, A. Introduction to Percolation Theory, 2nd Revised ed.; London: Taylor & Francis, **2003**; Chapter 5, p 89.
38. Alwarappan, S.; Erdem, A.; Liu, C.; Li, C. Z. *J. Phys. Chem. C.* **2009**, *113*, 8853.
39. Liao, K.; Li, S. *Appl. Phys. Lett.* **2001**, *79*, 4225.
40. Daniels, C.; Horning, A.; Phillips, A.; Massote, D. V. P.; Liang, L. B.; Bullard, Z.; Sumpter, B. G.; Meunier, V. *J. Phys.-Condes. Matter.* **2015**, *27*, 373002.